Density functional study of the electronic structure and lattice dynamics of $SrCl_2$

2010 J. Phys.: Condens. Matter 22 445402

(http://iopscience.iop.org/0953-8984/22/44/445402)

IOP Publishing
Journal of Physics: Condensed Matter
J. Phys.: Condens. Matter **22** (2010) 445402 (6pp)
doi:10.1088/0953-8984/22/44/445402

Density functional study of the electronic structure and lattice dynamics of $SrCl_2$

V Kanchana[1,2,6], **G Vaitheeswaran**[1,3], **P Souvatzis**[4], **O Eriksson**[4]
and S Lebègue[5]

[1] Applied Materials Physics, Department of Materials Science and Engineering,
Royal Institute of Technology (KTH), Brinellvägen 23, 100 44 Stockholm, Sweden
[2] Department of Physics, Indian Institute of Technology Hyderabad, Ordnance Factory Estate,
Yeddumailaram 502 205, Andhra Pradesh, India
[3] Advanced Centre of Research in High Energy Materials (ACRHEM), University of
Hyderabad, Gachibowli, Hyderabad 500 046, Andhra Pradesh, India
[4] Department of Physics and Astronomy, Uppsala University, Box 516, SE-751 20, Uppsala,
Sweden
[5] Laboratoire de Cristallographie, Résonance Magnétique et Modélisations (CRM2, UMR
CNRS 7036) Institut Jean Barriol, Nancy Université, BP 239, Boulevard des Aiguillettes
54506 Vandoeuvre-lès-Nancy, France

E-mail: kanchana@iith.ac.in

Received 16 August 2010, in final form 12 September 2010
Published 22 October 2010
Online at stacks.iop.org/JPhysCM/22/445402

Abstract
A theoretical study of the structural, electronic, optical and lattice dynamical properties of $SrCl_2$ in the cubic fluorite structure has been performed using first-principles calculations. The calculated ground state and elastic properties are in good agreement with the experiments. The calculated band gap is underestimated within the generalized gradient approximation for the exchange and correlation functional. GW calculations have been performed in order to improve the band gap and good agreement with the experiment is obtained. The phonon dispersion relations are discussed in detail in addition to the ground state and elastic properties. Also, the optical properties are computed with DFT corrected by the GW approximation.

(Some figures in this article are in colour only in the electronic version)

1. Introduction

Alkaline-earth halides crystallizing in the fluorite type structure such as CaF_2, SrF_2, BaF_2 and $SrCl_2$ exhibit fast-ion conduction at high temperatures [1, 2] and have attracted growing interest due to their technological importance in the field of solid state ionics [3]. $SrCl_2$, which is studied in this paper, has the unique distinction of being the only divalent metallic chloride crystallizing in the cubic fluorite structure without an established temperature dependent phase transition [4]. $SrCl_2$ exhibits superionic properties like other fluorite structure based compounds and these are widely studied by different experimental probes and theoretical models [5]. An interesting feature of this compound is the strong temperature dependence of the elastic constants [6], which is related to the superionic transition state. Considerable experimental and theoretical work involving structural, elastic and optical properties under ambient and high pressure is available for CaF_2, SrF_2 and BaF_2 [7–9]. Like all the fluorite type dihalides, $SrCl_2$ is also expected to undergo a structural phase transition to an orthorhombic structure [10]. Excited state emission spectra and luminescence properties of $SrCl_2$ have been investigated by several authors [11–14]. Lauer *et al* have determined the elastic constants experimentally using ultrasonic pulse echo technique [15]. Recently, a full-potential linear muffin-tin orbital method has been used to investigate the electronic structure of $SrCl_2$ leading to the determination of ground state and elastic properties [16]. The phonon dispersion curves, infrared and Raman spectra of $SrCl_2$ were studied a long time ago [18]. Phonon dispersion curves of $SrCl_2$ have been measured at room temperature in the [001], [110], [111] directions using the inelastic neutron scattering technique [19]. Structural and optical properties of $SrCl_2$ have been recently

---

[6] Author to whom any correspondence should be addressed.

studied theoretically using the full-potential linear augmented plane wave method [20].

One of the goals of the present work has been to explore the lattice dynamics of $SrCl_2$ theoretically using first-principles density functional calculations, in order to provide detailed information about the phonon frequencies of $SrCl_2$. In addition efforts were made to improve the band gap of $SrCl_2$ as compared to the earlier calculations [16, 20], by employing the GW approximation. From these more refined calculations, we have obtained the frequency dependent dielectric function. The rest of the paper is organized in the following manner. Section 2 deals with the computational details. Results and discussion are given in section 3 and finally section 4 concludes the paper.

2. Computational details

To perform the calculations, we have used VASP (Vienna *Ab Initio* Simulation Package) [22, 23], implementing the projector augmented wave (PAW) method [24] within density functional theory [25, 26]. The Perdew–Burke–Ernzerhof [27] variant of the generalized gradient approximation (GGA) was used for the exchange–correlation potential. A cut-off of 308 eV was used in the calculations. Total energies were calculated as a function of volume, for a (13, 13, 13) k-mesh, and are fitted to the Birch equation of state [28] to obtain the ground state properties. Elastic constants are calculated using volume conserving strains as outlined in [29]. We have relaxed the internal coordinates of the strained unit cell to arrive at the elastic constants.

The phonon dispersion of $SrCl_2$ was performed with the direct force method [30], where the force constant matrices are retained through a series of force calculations. In these calculations Methfessel–Paxton smearing of 0.2 eV was used together with a $6 \times 6 \times 6$ Monkhorst–Pack k-point grid. The supercell used was obtained by increasing the cubic primitive cell three times along the three primitive lattice vectors, resulting in a 81-atom supercell. Moreover, since DFT has difficulties in treating excited states, and in particular the band gap, which is usually underestimated by LDA or GGA, we have used the GW approximation (GWA) [32, 33] to obtain the band gap of $SrCl_2$. In the framework of the GW approximation, the following quasiparticle equation is solved:

$$(T + V_{\mathrm{ext}} + V_{\mathrm{h}})\psi_{\mathbf{k}n}(\mathbf{r}) + \int \mathrm{d}^3 r' \Sigma(\mathbf{r}, \mathbf{r}', E_n(\mathbf{k}))\psi_{\mathbf{k}n}(\mathbf{r}') \\ = E_n(\mathbf{k})\psi_{\mathbf{k}n}(\mathbf{r})$$

with T being the kinetic energy operator, V_{ext} the external potential due to the ion cores, and V_{h} the Hartree potential. Also, Σ is the self-energy operator, and $E_n(\mathbf{k})$ and $\psi_{\mathbf{k}n}(\mathbf{r})$ are respectively the quasiparticle energy and wavefunction. Then, the self-energy operator is written as the product of the Green's function times the screened Coulomb interaction W, which gives the so-called GW approximation. Finally, the GW quasiparticle eigenvalues are obtained as a correction of the DFT eigenvalues $\epsilon_n(\mathbf{k})$ such that [34]:

$$\mathrm{Re}\, E_n(\mathbf{k})) = \epsilon_n^{\mathrm{DFT}}(\mathbf{k}) + Z_{n\mathbf{k}} \\ \times [\langle \Psi_{\mathbf{k}n}^{\mathrm{DFT}} |\, \mathrm{Re}\, \Sigma(\mathbf{r}, \mathbf{r}', \epsilon_n(\mathbf{k}))|\Psi_{\mathbf{k}n}^{\mathrm{DFT}}\rangle \\ - \langle \Psi_{\mathbf{k}n}^{\mathrm{DFT}} | V_{xc}^{\mathrm{DFT}}(r)|\Psi_{\mathbf{k}n}^{\mathrm{DFT}}\rangle].$$

Table 1. Calculated GGA values of lattice constant, a, expressed in Å, bulk modulus, B_0, in GPa for $SrCl_2$, compared with experiment.

	a	B_0
Present	7.038	33
Expt	6.9744[a]	34.3[b]
Other theory	6.80[c], 7.042[d], 7.032[e]	37.2[d], 35.3[e]

[a] Room temperature value from [21].
[b] From elastic constants of [15].
[c] LAPW calculations using LDA of [31].
[d] LAPW calculations using GGA of [20].
[e] FP-LMTO calculations using GGA of [16].

The QP renormalization factor $Z_{n\mathbf{k}}$ corresponds to

$$Z_{n\mathbf{k}}^{\mathrm{DFT}} = \left[1 - \langle \Psi_{\mathbf{k}n}^{\mathrm{DFT}} | \frac{\partial}{\partial \omega} \mathrm{Re}\, \Sigma(\mathbf{r}, \mathbf{r}', \epsilon_n(\mathbf{k}))|\Psi_{\mathbf{k}n}^{\mathrm{DFT}}\rangle\right]^{-1}.$$

We have used the GW approximation implemented in the code VASP [35], which gives similar results to earlier GW implementations within the PAW formalism [36, 37]. To converge our calculation, 100 bands were used for the summation over bands in the calculation of the polarizability and the self-energy, and a cut-off of 150 eV was used for the size of the polarizability matrices.

3. Results

3.1. Structural and electronic properties

As a first step, the equilibrium lattice parameter has been computed by minimizing the total energy calculated for different volumes by using the Birch equation of state [28]. The calculated lattice constant obtained within the GGA to the exchange–correlation potential slightly overestimates the experimental value at room temperature by 0.78%. This value is also in accord with the earlier results obtained using the FP-LMTO method [16]. The bulk modulus is also calculated at the theoretical volume and it is also in good agreement with the experiments. The results are compared with the available experimental and theoretical values in table 1.

$SrCl_2$ is an indirect band gap insulator, whose band gap has been reported to be 5.18 eV in the earlier theoretical investigations [16]. This is substantially lower than the 7.5 eV reported experimentally [11]. Hence it is worth making efforts to improve the band gap before we proceed with the optical studies.

In the present study, GW calculations have been performed in order to improve the band gap along the high-symmetry directions and they are shown in figure 1. The lower-lying bands are predominantly the Sr p and Cl s-like states. These states are lying deep in the energy range of −15 to −12 eV. The conduction band states are dominated by Sr d-like states with a mixture of Cl d and Sr s-like states. From the band structure it appears that the top of the valence band is at the X point and the bottom of the conduction band lies at the Γ point. The values of band gap using the GGA/GW approximations at the Γ, X and W points are found to be 5.7/7.8, 5.5/8.0 and 6.4/8.8 eV respectively. The indirect band gap measured in the

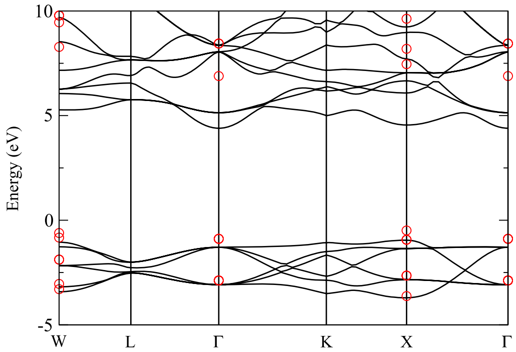

Figure 1. Band structure of $SrCl_2$ at the theoretical lattice constant (GGA, full lines; GW, dots). The coordinates (in reciprocal space) of the high-symmetry points are the following: W (0.5 0.75 0.25); L (0.5 0.5 0.5); Γ (0 0 0); K (0.75 0.375 0.375); X (0.5 0.5 0.0).

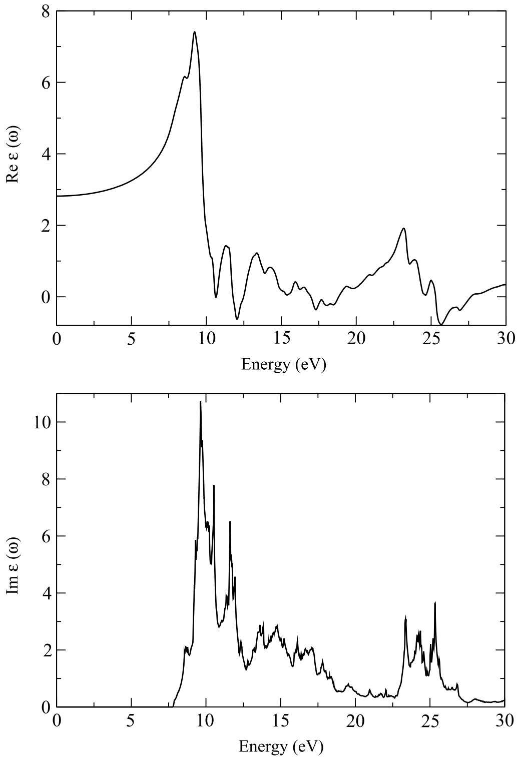

Figure 2. Real and imaginary parts of the dielectric function computed with a scissor shift obtained from GW calculations.

X–Γ direction is 7.8 eV using the GW approximation and it is in excellent agreement with the experimentally reported value of 7.5 eV [11]. From the band structure, one observes that the valence band is composed predominantly by Cl p states with a band width of 2.75 eV with the GGA and 3.2 eV with the GW approximation. The deep-lying Cl s-like states are not shown in the figure.

The ordering of the bands is preserved when going from DFT to GW, and therefore the GW correction can be seen to a first approximation as a rigid shift of the conduction bands of $SrCl_2$. This fact will be used to obtain the correct optical spectra (see below).

3.2. Optical properties

The optical properties of matter can be described by means of the transverse dielectric function $\epsilon(\omega)$. This comprises two contributions, namely the interband and intraband transitions. The contributions from intraband transition find importance only in metals. The interband transitions can further be split into direct and indirect transitions. Here we neglect the indirect interband transition, which involves scattering of phonons and is expected to contribute only little to $\epsilon(\omega)$. To calculate the direct interband contributions to the imaginary part of the dielectric function, one must sum up all possible transitions from occupied to unoccupied states.

The real part of the frequency dependent dielectric function can be derived from the imaginary part using the Kramers–Kronig relations. The knowledge of both the real and imaginary parts of the frequency dependent dielectric function allows the calculation of important optical functions such as refractive index, reflectivity and absorption coefficients. Optical property calculations need a dense mesh of uniformly distributed k-points. Hence the Brillouin zone integration was performed with a $16 \times 16 \times 16$ k-point mesh in the Brillouin zone.

Figure 2 displays the real and imaginary parts of the dielectric function of $SrCl_2$. A scissor-operator correction of 2.1 eV, corresponding to the GW correction at the Γ point, has been applied in order to correct the deficiency of DFT concerning the band gap. By analysing the curve, it is quite clear that the threshold energy of the dielectric function occurs at around 8 eV. This corresponds to direct transitions at the high-symmetry points X and Γ between the highest valence and lowest conduction bands, and is known as the fundamental absorption edge. Beyond these points, the curve increases rapidly, as the number of points contributing to $\mathrm{Im}\,\epsilon(\omega)$ increases abruptly. The main peak in the spectra is situated at around 10 eV. This peak might have evolved from some direct transitions at some other points in the Brillouin zone, such as the L point. The main peak is further followed by three other peaks located around 12, 15 and 23 eV. Using our calculated band structure it would be worthwhile to identify the interband transitions that are responsible for the $\mathrm{Im}\,\epsilon(\omega)$. The first structure can be assigned to the direct transitions along the (L–Γ) directions. The second one is primarily due to the (W–W) transition with contributions of direct transitions along (X–W) direction, while the last structure comes from direct transition along the (W–L) direction. It can be clearly seen that the Cl p states and Sr d states play a major role in the optical transitions as initial and final states respectively. The zero-frequency limit of the real part of the dielectric function has a value of 2.8, which corresponds, as expected, to a value for a large-band-gap insulator.

3.3. Elastic properties

The elastic constants of solids provide a link between the mechanical and dynamical behaviour of crystals and provide important information concerning the nature of forces operating in solids. In particular, they provide information

Table 2. Calculated elastic constants, shear modulus G, Young's modulus E, all expressed in gigapascals, and Poisson's ratio ν for $SrCl_2$. Results from the present study refer to the calculated equilibrium volume.

	C_{11}	C_{12}	C_{44}	G	E	ν
Present	66	16	12	17	44	0.276
Expt[a]	70.2	16.4, 17.3	9.72	16.6	42.9	0.292
Others	70.5[b], 66.9[c]	20.5[b], 19.6[c]	14.2[b], 9.9[c]	18.5[b], 15.4[c]	47.6[b], 42.9[c]	0.4[b], 0.310[c]

[a] Data at 195 K, from [15]. [b] LAPW calculations using GGA of [20]. [c] FP-LMTO calculations using GGA of [16].

on the stability and stiffness of materials and their calculation requires precise methods. In the present work elastic constants have been computed in a manner similar to our earlier work [16] and are tabulated in table 2.

The calculated elastic constants, Young's modulus, shear modulus and Poisson's ratio obtained in the present study are in good agreement with the available experimental and earlier theoretical work. The value of C_{44} is slightly overestimated when compared with the experimental value. In addition we would like to mention as a point of caution that the experimental values quoted in the table are obtained at 195 K, whereas the calculated values pertain to 0 K. Finite temperature generally tends to reduce the elastic constants. Consequently, we would expect the experimental values at low temperature to be somewhat higher then the quoted values and thereby we could find theoretical values to agree better with the experimental values.

A simple relationship which empirically relates the plastic properties of materials with the elastic moduli was proposed by Pugh [17]. The shear modulus G represents the resistance to plastic deformation whereas the bulk modulus B represents the resistance to fracture. A high B/G ratio is associated with ductility whereas a low value corresponds to a brittle nature. The critical value of B/G which separates ductile from brittle materials is around 1.75 (i.e., if the B/G value is greater than 1.75 the material behaves in a ductile manner, otherwise the material behaves in a brittle manner). In the case of $SrCl_2$ the B/G ratio is found to be around 1.90, classifying this material as ductile.

In addition, we have calculated the longitudinal, v_l, the shear, v_s, and the average, v_m, sound velocities in the (100) and (111) directions of $SrCl_2$, through the relations [40]

$$v_l^{(100)} = \sqrt{\frac{C_{11}}{\mathcal{D}}}, \qquad v_s^{(100)} = \sqrt{\frac{C_{44}}{\mathcal{D}}}, \tag{1}$$

$$v_l^{(111)} = \sqrt{\frac{C_{11} + 2C_{12} + 4C_{44}}{3\mathcal{D}}}, \qquad v_s^{(111)} = \sqrt{\frac{C_{11} - C_{12} + C_{44}}{3\mathcal{D}}}, \tag{2}$$

$$v_m = \tfrac{1}{3}v_l + \tfrac{2}{3}v_s, \tag{3}$$

where $\mathcal{D}$ denotes the density of mass. The results are listed in table 3.

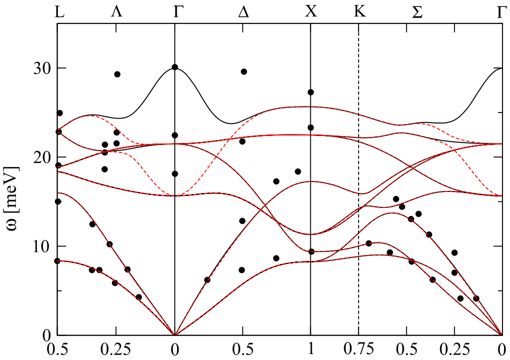

Figure 3. Theoretical phonon dispersion, solid black line and red dashed line, together with experimental data [19], black circles. Here the solid black line is the calculation where the LO–TO splitting has been taken into account by means of equation (4), whereas the red dashed line displays the results of the calculation where no LO–TO splitting has been imposed.

Table 3. Longitudinal, v_l, shear, v_s, and average, v_m, sound velocities in km s^{-1} for $SrCl_2$ in the (100) and (111) directions, calculated through equations (1)–(3).

	v_l	v_s	v_m
Present (100)	4.67	2.02	2.90
Present (111)	4.04	2.61	3.08
Expt (100)[a]	4.79	1.78	2.78
Expt (111)[a]	3.93	2.61	3.05

[a] The experimental data are taken from [15].

3.4. Phonon dispersion of $SrCl_2$

The calculated phonon dispersion and phonon density of states are shown in figures 3 and 4 respectively. We do not find any imaginary phonon frequency in the dispersion curve. This support the dynamical stability of the compound in the fluorite structure which is also evident from the positive values of the elastic constants which was discussed earlier. Here the best agreement between theory and experiment is primarily found for the acoustic phonon branches, whereas there are substantial discrepancies at the optical modes. These discrepancies can of course be ascribed to the tendency of the GGA approximation to underbind, resulting in slightly underestimated theoretical optical frequencies at the Γ and X points, which in principle could be changed to overestimations if the LDA approximation were to be employed [38]. However, the more likely cause of the discrepancies is size effects due to the limited size of the supercell used in the calculation. One of the more pronounced size effects is the degeneracy between the longitudinal-optical and transverse-optical phonon modes at $\mathbf{q} = 0$; see the red dashed curve in figure 3. This is degeneracy is due to the incorrect treatment of the infinite range dipole–dipole

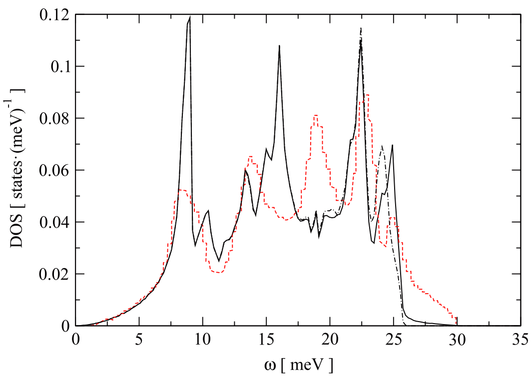

Figure 4. Theoretical phonon density of states solid black line and dashed–dotted line, together with experimental data [19], red dashed line. Here the solid black line is the calculation where the LO–TO splitting has been taken into account by means of equation (4), whereas the black dashed–dotted line displays the results of the calculation where no LO–TO splitting has been imposed. Observe that both the experimental and theoretical density of states, $g(\omega)$, has been normalized so that $\int_0^\infty g(\omega)\,\mathrm{d}\omega = 1$.

interaction, and is only removed if an infinite size supercell is used, or if non-analytical corrections to the dynamical matrix are included in an ad hoc manner.

The splitting between the longitudinal- and transverse-optical phonon modes at $\mathbf{q} = 0$ (LO–TO splitting) was taken into account by means of the non-analytical dipole–dipole interaction correction to the dynamical matrix, given by the expression found by Parlinski *et al* [39],

$$\mathcal{D}^{\mu\nu}_{mn}(\mathbf{q})_{\mathrm{corr}} = \frac{4\pi e^2}{V\sqrt{M_\mu M_\nu}} \frac{(\bar{\bar{Z}}^{\mu}\mathbf{q})_m(\bar{\bar{Z}}^{\nu}\mathbf{q})_n}{\mathbf{q}\bar{\bar{\epsilon}}_\infty\mathbf{q}} \mathrm{e}^{-\mathrm{i}\mathbf{G}(\mathbf{b}_\mu-\mathbf{b}_\nu)}\mathrm{e}^{-\mathbf{q}^2/\rho^2}. \tag{4}$$

Here m, n are Cartesian coordinate indices, V the volume of the primitive cell and M_μ, $\bar{\bar{Z}}^{\mu}$ is the mass respectively Born-effective-charge matrix of atom μ, which is placed at the relative atomic coordinate $\mathbf{b}_\mu$. Furthermore, $\bar{\bar{\epsilon}}_\infty$ is the static infinite wavelength dielectric matrix, $\mathbf{G}$ is the reciprocal lattice vector at which $\mathbf{q}$ is centred and ρ is a free damping parameter, which is used to suppress the correction term as $|\mathbf{q}| > 0$.

Since it was beyond the scope of this study to calculate the Born-effective-charge matrices and the dielectric matrix, $\bar{\bar{\epsilon}}_\infty$, and since we could not find these constants in the literature, they were treated as parameters and chosen in such a way that they reproduced the LO phonon mode at $\mathbf{q} = 0$. The Born-effective-charge matrices used for the Sr and Cl atoms were $Z^{\mathrm{Sr}}_{ij} = 2\delta_{ij}$ and $Z^{\mathrm{Cl}}_{ij} = -\delta_{ij}$, the dielectric matrix used was $\epsilon^{ij}_\infty = 1.35\delta_{ij}$ and the damping parameter used was $\rho = 0.0425$ Å^{-1}.

The effect of the inclusion of the non-analytical correction can be clearly seen in figure 3 (solid black line), as it completely removes the degeneracy between the LO and TO modes at the Γ point. Furthermore, from the phonon density of states displayed in figure 4, it becomes evident that LO–TO splitting only affects the spectrum at frequencies of $\gtrsim$25 meV.

4. Conclusions

A theoretical study of the structural, electronic, optical and lattice dynamical properties of SrCl$_2$ has been carried out using the first-principles calculations. The calculated properties are found to be in good agreement with the experiments. In addition, GW calculations have been performed with the aim of improving the band gap, which is usually underestimated with the LDA or the GGA approximation for the exchange–correlation potential. Optical properties and lattice dynamics of SrCl$_2$ are also presented in detail in addition to the ground state and elastic properties.

Acknowledgments

SL acknowledges financial support from ANR PNANO grant No ANR-06-NANO-053-02 and computer time using HPC resources from GENCI-CCRT/CINES (grant 2010-085106). SL is grateful to C Jelsch for technical help. OE is grateful to VR, SSF and ERC.

References

[1] Nagel L E and O'Keefe M 1973 *Fast Ion Transport in Solids* ed W Van Gool (Amsterdam: North-Holland) p 165
[2] Reau J M, Fedorov P P, Rabardel L, Matar S F and Hagenmuller P 1983 *Mater. Res. Bull.* **18** 1235
[3] Elaine M, Tom G and Kurt L 2001 *J. Phys. Chem. Solids* **62** 1117
[4] Mark H and Tolksdorf S 1925 *Z. Phys.* **33** 681
[5] Boyce J B and Huberman B A 1979 *Phys. Rep.* **51** 189
[6] Catlow C R A, Comins J D, Germano F A, Harley R T and Hayes W 1978 *J. Phys. C: Solid State Phys.* **11** 3197
[7] Dubinin A, Winkler B, Knorr K and Milman V 2004 *Eur. Phys. J.* B **39** 27
[8] Schnalzl K, Strauch D and Schober H 2003 *Phys. Rev.* B **68** 144301
[9] Schmalzl K 2007 *Phys. Rev.* B **75** 014306
[10] Brixner L H 1976 *Mater. Res. Bull.* **11** 1453
[11] Sugiura C 1974 *Phys. Rev.* B **9** 2679
[12] Tabakova V 1993 *Solid State Commun.* **87** 135
Tabakova V 1994 *Mater. Chem. Phys.* **38** 91
[13] Pan Z, Ning L, Cheng B M and Tanner P A 2006 *Chem. Phys. Lett.* **428** 78
[14] Grimm J, Wenger O S, Kramer K W and Gudel H U 2007 *J. Lumin.* **126** 590
[15] Lauer H V Jr, Solberg K A, Kühner D H and Bron W E 1971 *Phys. Lett.* A **35** 219
[16] Kanchana V, Vaitheeswaran G and Svane A 2008 *J. Alloys Compounds* **455** 480
[17] Pugh S F 1954 *Phil. Mag.* **45** 823
[18] Denham P A, Morse P L R and Wilkson G R 1973 *J. Phys. C: Solid State Phys.* **6** 2066
[19] Sadoc A, Moussa F and Pepy G 1976 *J. Phys. Chem. Solids* **37** 197
[20] Benmimoun Y, Bouhemadou A, Khenata R, Reshak A H, Amrani B, Ameri M and Baltache H 2008 *Eur. Phys. J.* B **61** 165
[21] Wyckoff R W G 1982 *Crystal Structures* 2nd edn, vol 1 (New York: Interscience)
[22] Kresse G and Furthmüller J 1996 *Phys. Rev.* B **54** 11169
[23] Kresse G and Joubert D 1999 *Phys. Rev.* B **59** 1758
[24] Blöchl P E 1994 *Phys. Rev.* B **50** 17953
[25] Honenberg P and Kohn W 1964 *Phys. Rev.* **136** B864
[26] Kohn W and Sham L 1965 *Phys. Rev.* **140** A1133

[27] Perdew J P, Burke K and Ernzerhof M 1996 *Phys. Rev. Lett.* **77** 3865
[28] Birch F J 1938 *J. Appl. Phys.* **9** 279
[29] Kanchana V, Vaitheeswaran G, Svane A and Delin A 2006 *J. Phys.: Condens. Matter* **18** 9615
[30] Parlinski K 2007 *J. Phys.: Conf. Ser.* **92** 012009
[31] Válgoma J A, Perez-Mato J M, Garcia A, Schwarz K and Blaha P 2002 *Phys. Rev.* B **65** 134104
[32] Hedin L 1965 *Phys. Rev.* **139** A796
[33] Hedin L and Lundquist S 1969 *Solid State Physics* vol 23, ed H Ehrenreich, F Seitz and D Turnbull (New York: Academic) p 1
[34] Onida G, Reining L and Rubio A 2002 *Rev. Mod. Phys.* **74** 601
[35] Shishkin M and Kresse G 2006 *Phys. Rev.* B **74** 035101
[36] Lebègue S, Arnaud B, Alouani M and Blöchl P E 2003 *Phys. Rev.* B **67** 155208
[37] Lebègue S, Alouani M, Arnaud B and Pickett W E 2003 *Europhys. Lett.* **63** 562
[38] Souvatzis P and Eriksson O 2008 *Phys. Rev.* B **77** 024110
[39] Parlinski K, Li Z Q and Kawazoe Y 1998 *Phys. Rev. Lett.* **81** 3298
[40] Ashcroft N W and Mermin N D 1976 *Solid State Physics* (London: Thomson Learning Inc.) p 447